

Frequency-Dependent Seismic Attenuation within the Hispaniola Island Region of the Caribbean Sea

by D. McNamara, M. Meremonte, J. Z. Maharrey, S-L. Mildore, J. R. Altidore, D. Anglade, S. E. Hough, D. Given, H. Benz, L. Gee, and A. Frankel

1 **Abstract** We determine frequency-dependent attenuation $1/Q(f)$ for the Hispaniola region using direct S and L_g waves over five distinct passbands from 0.5 to 16 Hz. Data consist of 832 high-quality vertical and horizontal component waveforms recorded on short-period and broadband seismometers from the devastating 12 January 2010 **M** 7.0 Haiti earthquake and the rich sequence of aftershocks. For the distance range 250–700 km, we estimate an average frequency-dependent $Q(f) = 224(\pm 27)f^{0.64(\pm 0.073)}$ using horizontal components of motion and note that $Q(f)$ estimated with L_g at regional distances is very consistent across vertical and horizontal components. We also determine a $Q(f) = 142(\pm 21)f^{0.71(\pm 0.11)}$ for direct S waves at local distances, ≤ 100 km. The strong attenuation observed on both vertical and horizontal components of motion is consistent with expectations for a tectonically active region.

Online Material: To be set by the editorial office.

Introduction

In this study we focus on the attenuation characteristics of the Caribbean island of Hispaniola and the surrounding region, ranging from Jamaica and Cuba in the west to Puerto Rico in the east (Fig. 1). The island of Hispaniola, which comprises the countries of Haiti and the Dominican Republic, is mountainous with maximum elevations of nearly 4000 m and lies at the complex boundary between the North American and Caribbean tectonic plates (Fig. 1). Relative plate motion is approximately 20 m/yr with Hispaniola at the transition zone between a subduction zone to the east (Fig. 1, Puerto Rico trench) and a dominantly strike-slip plate boundary to the west (Fig. 1, Cayman trench) (Bird, 2003; **2** Manaker *et al.*, 2008). Two major crustal transpressional strike-slip fault systems—the Septentrional fault to the north and the Enriquillo Plantain Garden fault to the south (Manaker *et al.*, 2008; Calais, *et al.*, 2010)—run roughly east-west across Hispaniola posing a significant earthquake hazard (Prentice, *et al.*, 2010; Frankel *et al.*, 2010; Mann *et al.*, 1984). On 12 January 2010, an M_w 7.0 earthquake occurred in this region killing more than 230,000 people in the city of Port-au-Prince, Haiti, and causing submarine landslides that resulted in the production of local tsunami inundation (Hornbach *et al.*, 2010). The earthquake was the largest to strike the southern part of Hispaniola since 3 June 1770 (Calais *et al.*, 2010) and was due to a complex rupture process involving slip on multiple faults (Hayes *et al.*, 2010). In the year following the **M** 7.0 earthquake, numerous after-

shocks have occurred with a diffuse distribution of hypocenters that are located primarily at the western margin of the region of significant slip, suggesting that most of these events reflect triggered slip on minor faults rather than defining the mainshock coseismic rupture zone (Hayes *et al.*, 2010).

Historically, only a small number of recordings of moderate-to-large magnitude earthquakes (**M** > 5) at local distances were available in the Hispaniola region, limiting the determination of ground-motion relations for magnitudes and distances for engineering interest. In this study, we utilize the Haiti **M** 7.0 mainshock and a rich sequence of aftershocks to solve for frequency-dependent attenuation $Q(f)$ using the seismic phases L_g at regional distances and direct S waves at local distances. $Q(f)$ is an important physical parameter and is required for successful simulation of strong ground motion using techniques such as semiempirical modeling (Joshi and Midorikawa, 2004), composite source modeling (Zeng *et al.*, 1994), and stochastic simulation (Boore, 1983).

The L_g phase propagates with a group velocity of about 3.5 km/s, the average crustal shear-wave velocity, and is commonly observed as the dominant phase on high-frequency seismograms at regional distances (e.g., Isacks and Stephens, 1975; McNamara and Walter, 2001). L_g is generated by **4** a superposition of higher-mode surface waves (Oliver and Ewing, 1957; Knopoff *et al.*, 1973) or as multiply-reflected

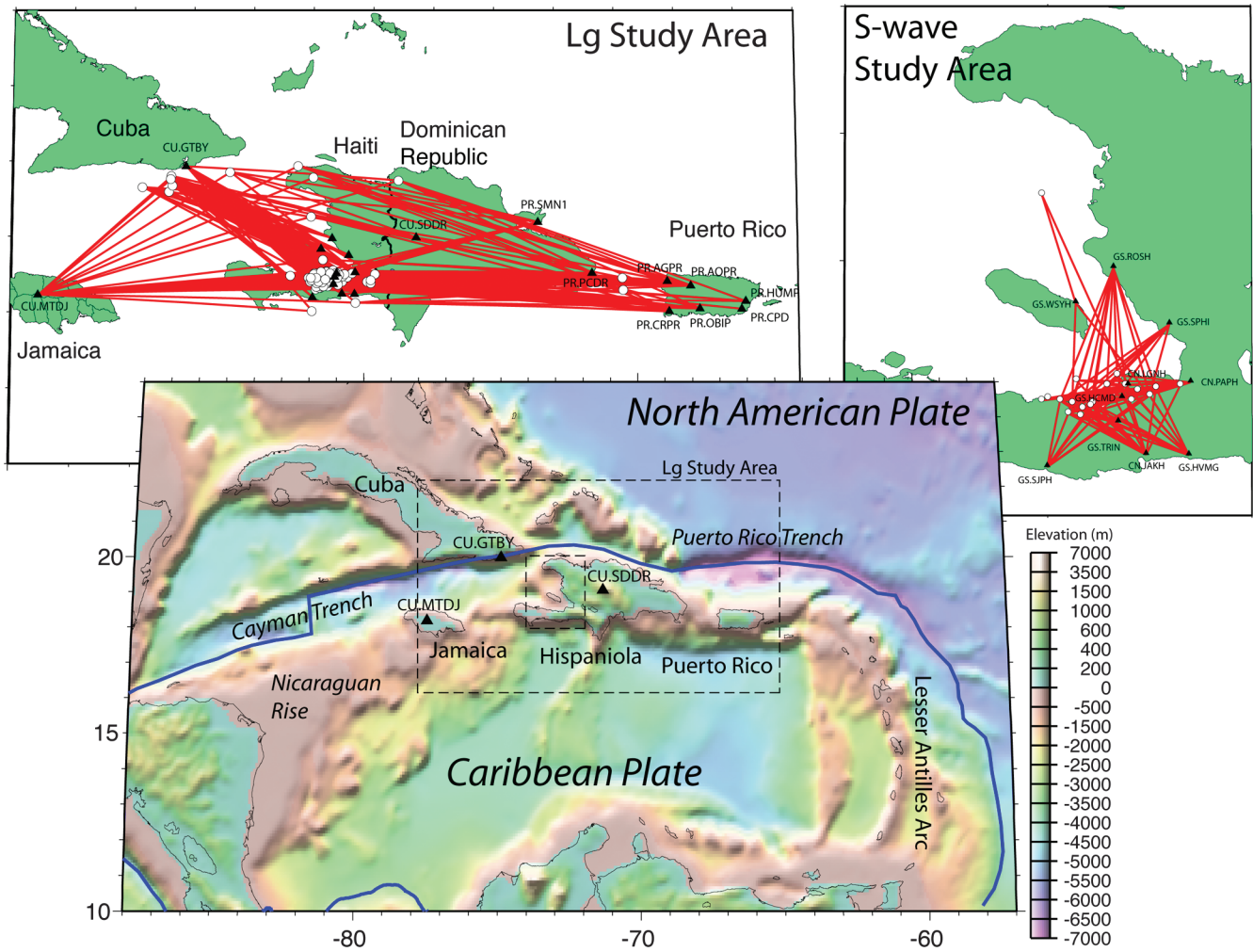


Figure 1. Tectonic setting and study area maps showing the tectonic plate boundary (blue lines) between the North American and Caribbean plates (Bird, 2003). The small inset boxes (dashed lines) are the L_g and S -wave Q study areas. The L_g study area has 749 L_g propagation paths (red lines) from 125 shallow ($h \leq 15$ km) earthquakes (white circles) (see Table S1, available in the electronic supplement to this paper) recorded at 25 short-period and broadband seismic stations (black triangles) (see Table S2, available in the electronic supplement to this paper). The S -wave study area shows 90 S -wave propagation paths (red lines) from 22 shallow ($h \leq 15$ km) earthquakes (white circles) (see Table S1, available in the electronic supplement to this paper) recorded at 10 short-period and broadband seismic stations (black triangles) (see Table S2, available in the electronic supplement to this paper).

shear energy in a crustal waveguide (Press and Ewing, 1952; Gutenberg, 1955). Consequently, L_g provides a good measure of path-averaged crustal properties such as shear-wave velocity and attenuation. L_g amplitude is sensitive to lateral heterogeneity in the crust due to varying tectonic environments (Erickson, et al., 2004). L_g attenuation is higher for tectonically active regions than for stable continental interiors (Frankel et al., 1990; Atkinson et al., 1992; Xie and Mitchell, 1993; McNamara et al., 1996; Benz et al., 1997; McNamara, 2000; Ottemoller, 2002). Several mechanisms have been proposed to explain these observations: differences in crustal heterogeneity leading to differences in absorption of high-frequency energy (Aki, 1980), differences in crustal temperature (Frankel et al., 1990), and variations in crustal structures that control elastic wave propagation (Gregersen, 1984; Kennett, 1986). L_g is generally observed to propagate ineffi-

ciently or to be completely absent in thin oceanic crust (Kennett, 1986; McNamara et al., 2001; Zhang and Lay, 1995).

Numerous researchers have estimated $Q(f)$ for the Earth's crust throughout the world (Aki, 1980; Campillo et al., 1985; Chavez and Priestly, 1986; Frankel et al., 1990; Atkinson and Mereu, 1992; McNamara et al., 1996; Benz et al., 1997). The frequency-dependent quality factor $Q(f)$ is commonly modeled using a power law of the form

$$Q(f) = Q_0(f/f_0)^\eta, \quad (1)$$

where f_0 is a reference frequency (generally 1 Hz), Q_0 is Q at the reference frequency, and η is assumed to be constant over the frequencies of interest. In this study we use data from broadband instruments to determine $Q(f)$ in the Hispaniola region and compare the results with attenuation determined for other regions.

Q Inversion Methods

Data Selection and Amplitude Measurement

L_g and S -wave amplitudes used in the inversion were restricted to stations that recorded at least two earthquakes and earthquakes recorded by at least two stations. In addition to visual inspection, we required a signal-to-noise root mean square (RMS) amplitude ratio greater than two, where the noise amplitude is taken from the P coda rather than preceding the P wave. This step eliminated very few paths, because L_g is generally the dominant arrival on regional seismograms, and ensured observations where L_g is present at all distances. The goal was to eliminate paths crossing L_g -blocking structures, such as abrupt crustal thickness transitions from continental to oceanic crust, that would bias the regional Q estimate (McNamara and Walter, 2001). The RMS amplitude for L_g was windowed from 3.6 to 3.0 km/s, direct S from 4.8 to 3.6 km/s and the P coda was windowed from 5.8 to 4.8 km/s. The window for the P coda was chosen to select the scattered energy between faster crustal P waves (P_g) and slower upper mantle S waves (S_n). Regional and local waveforms that passed the signal-to-noise criteria were further processed to obtain L_g and direct S -wave spectral amplitude measurements. This included deconvolution of the instrument response transfer function from the band-pass-filtered seismogram. Finally, the RMS amplitude of L_g and S were measured in five one-octave passbands with center frequencies of 0.75, 1.5, 3, 6 and 12 Hz. After applying the earthquake and waveform selection criteria to over 2000 regional seismograms, nearly 850 high-quality L_g and S -wave waveforms remained: from 125 events recorded at 25 stations. Figure 2 shows an example of well-recorded S -wave and L_g arrivals that passed the data selection criteria for an earthquake (20 March 2010, 18 h 8 m 8.72 s) located off the southeastern shore of Cuba (19.67 N, 75.33 W; 14 km depth; and M_w 5.6) (Table S2, available in the electronic supplement to this paper) recorded at the portable aftershock station GS.WSYH.00.EHE ($\Delta = 275.4$ km). (Fig. 1b; Table S1, available in the electronic supplement to this paper). Seismic velocity windows and phases are labeled in Figure 2 at the five filtered passbands used in this study. In general, S -wave and L_g amplitudes decrease with increasing frequency content. We also observe measurable L_g amplitudes (Fig. 2) despite significant oceanic paths (Fig. 1; McNamara and Walter, 2001). Additional filtered seismograms are available as an electronic supplement to this paper (Fig. S1).

Single Frequency Q Inversion

The inversion method used in this study to estimate $Q(f)$ is well known (Frankel *et al.*, 1990; McNamara *et al.*, 1996; McNamara, 2000; Erickson *et al.*, 2004) and described in detail by Benz *et al.* (1997). The observed amplitude A at frequency f for the j th earthquake recorded at the i th station can be modeled as

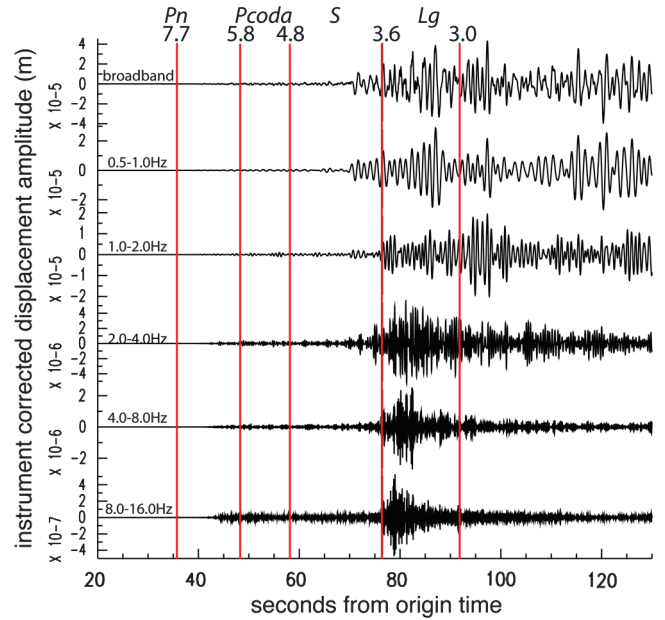


Figure 2. The 20 March 2010, 18 h 8 m 8.72 s earthquake located off the southeastern shore of Cuba (19.67 N, 75.33 W; 14 km depth; and M_w 5.6) recorded at the portable aftershock station GS.WSYH.00.EHE ($\Delta = 275.4$ km). Shown is the GS.WSYH.00.EHE (100 samples per second) component of the instrument corrected displacement seismogram. The seismogram is filtered in five passbands. Seismic velocity windows (red lines) and phases used in the data selection procedure are shown.

$$A_{ij}(f) = R_{ij}^{-\gamma} S_j(f) G_i(f) e^{-\pi f R_{ij} / Q\beta}, \quad (2)$$

where $S_j(f)$ is the source spectra, $G_i(f)$ is the site amplification, R_{ij} is the epicentral distance between the earthquake j and station i , γ is the exponent for geometrical spreading, Q is the quality factor at frequency f , and β is the average shear-wave velocity for the crust—3.5 km/s for this study. Taking the logarithm of equation (2) yields the following:

$$\ln A_{ij}(f) + \gamma \ln R_{ij} = \ln G_i(f) + \ln S_j(f) - \pi f R_{ij} / Q\beta. \quad (3)$$

When amplitude corrected for geometric spreading (the left side of equation 3) is plotted with respect to distance, the right side of equation (3) describes a line where the receiver (G_i) and source (S_j) terms control the intercept, and the Q term controls the slope. Using a dataset with many source-receiver pairs, a system of linear equations can be set up based on equation (3). The system of equations can be expressed as

$$\mathbf{Ax} = \mathbf{t}, \quad (4)$$

where \mathbf{A} is the system matrix made up of the parameter coefficients of equation (3), \mathbf{x} is a column vector containing the unknown source (S) and receiver (G) terms and the regional Q term, and the \mathbf{t} vector is comprised of the left hand side of equation (3). The system matrix \mathbf{A} is made up of mostly ones and zeros, with the last column listing a portion of the last

term of equation (3), $(\frac{-\pi f R_i}{\beta})$. We solve for each frequency independently, and the known variables are R , f , and β for each source–receiver pair. A singular value decomposition (SVD) inversion algorithm is then applied to solve for the unknown variables S_j and G_i , as well as a regionally averaged Q for a single frequency passband with center frequency f (e.g., Menke, 1980; Aster *et al.*, 2002).

13

Sensitivity of $Q(f)$ to Geometric Spreading

In developing attenuation models, we must determine if $Q(f)$ can be determined by assuming a single geometric spreading rate γ or if an epicentral distance dependence is indicated. Several previous studies have described the geometrical spreading function as a hinged-trilinear functional form, in which amplitude decay varies as a function of epicentral distance (Atkinson and Mereu, 1992; Atkinson and Boore, 1995). For example, Atkinson (2004) describes attenuation in eastern North America by parameterizing geometrical spreading as $R^{-1.3}$ to 70 km, as $R^{0.2}$ for 70–130 km, and $R^{-0.5}$ beyond 130 km. This parameterization is interpreted as reflecting changes in the dominant wave type. At close distances, the direct S waves dominate and the attenuation rate is steep, $R^{-1.3}$. At distances beyond 70 km, the postcritical reflections from the Moho discontinuity join the direct S waves, increasing energy levels and decreasing the attenuation rate, $R^{0.2}$. At regional distances, multiple refractions and reflections of the shear waves trapped in the crustal waveguide L_g dominate seismic records, and the attenuation rate changes to the commonly used form $R^{-0.5}$ (Frankel, 1991; McNamara *et al.*, 1996; Benz *et al.*, 1997). In an attenuation study in Puerto Rico, Motazedian and Atkinson (2005) found significant distance-dependent geometrical spreading and adopted a hinged-trilinear functional form specific to Puerto Rico, where geometrical spreading is described by R^{-1} , R^0 , and $R^{-0.5}$, with hinge points at 75 and 100 km.

15 Figure 3 shows the distribution of raw horizontal component L_g (BHE) and S -wave (BH1) amplitudes, measured in the 1–2 Hz frequency band as a function of distance. S -wave (green squares) and L_g (green circles) amplitudes for the **M 7.0** Haiti earthquake (20100112215310), recorded only at permanent stations, and an **M 4.2** (20100328071617), recorded by nearly all stations in the study, are also shown. We observe a significant amount of scatter. Amplitude variability is due to the range of magnitudes spanned by the dataset, variability in regional Q , site amplification, and possible errors in the instrument response transfer function. Earthquake magnitude variation will be absorbed into the source term (S) in equation (3), and any systematic amplitude contributions due to site response amplification and/or instrument response will be absorbed into the receiver term (G). Because we cannot separate site amplification from instrument response contributions, we are not able to interpret the receiver (G) term as being due to regional site amplification variations.

18
19 Both phase type and attenuation rate changes as a function of epicentral distance are clearly observed in Figure 3. In

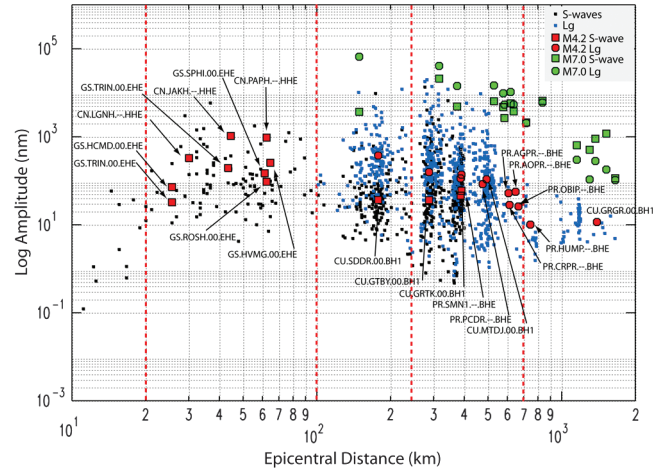


Figure 3. Raw 1–2 Hz horizontal component local S -wave (black squares) and regional L_g (blue squares) amplitudes from stations BHE and BH1 plotted as a function of distance. Also plotted are S -wave (green squares) and L_g (green circles) amplitudes for the **M 7.0** Haiti earthquake (20100112215310) recorded by permanent stations in the region and S -wave (red squares) and L_g (red circles) amplitudes for an **M 4.2** earthquake (20100328071617) recorded by both portable and permanent stations (Fig. 1a, b; see Table S2, available in the electronic supplement to this paper) in the study. Changes in slope at distances of 20, 250, and 700 km indicate changes in attenuation as a function of epicentral distance.

general, L_g is not well established and separate from crustal S waves in paths shorter than 100 km. At distances < 100 km, crustal S waves are the largest phase on the seismogram (Fig. 3, black squares). At distances from 100 to 250 km, L_g develops (Fig. 3, blue squares) while crustal S waves are still present. Beyond 250 km, body waves consist of small amplitude mantle head waves (S_n) and crustal L_g dominates the seismogram. Despite the scatter in Figure 3, we observe that the attenuation rate depends strongly on epicentral distance, with clear changes in slope at several hinge points. Observed raw amplitudes show significant changes in slope at distances of 20 km, 250 km, and 700 km (Fig. 3). This observation is consistent with observations made previously in other regions (Atkinson, 2004; Motazedian and Atkinson, 2005), although the hinge points in our dataset are unique to the crustal attenuation and velocity structure of the Hispaniola region.

P -Wave Velocity Structure

We analyzed the travel times of first arriving P waves in order to further investigate crust and upper mantle structure deduced from the distance-dependent L_g and S -wave amplitudes observed in Figure 3. This dataset yielded over 2000 travel times, which were assigned a quality factor from A to D, depending on the precision and confidence in the phase pick. Figure 4 shows the A and B quality travel times versus distance for 503 first arriving P waves plotted with a reducing velocity of 7.7 km/s. Clear changes in slope are observed at 200 km (Fig. 4, Xd) and 700 km (Fig. 4, Xm),

suggesting that three separate P phases are present in the dataset. A least-squares fit to travel times at distances up to 200 km results in a propagation velocity of 6.6 km/s and is most consistent with the crustal P_g phase. Travel times at distances of 200–700 km propagate at 7.7 km/s and are most consistent with the mantle head wave (P_n) while travel times at epicentral distances >700 km propagate at 8.3 km/s and are likely due to P waves that propagate at greater depths in the mantle (Fig. 4).

The crossover distance ($X_d = 200$ km) and intercept time ($T_i = 2.97$ s) determined from the least-squares fit to the mantle head-wave P_n (Fig. 4) can be used to uniquely determine crustal thickness from standard refraction seismology methods (Dobrin and Savit, 1988). Intercept time (T_i) is expressed by the following:

$$T_i = 2h \sqrt{\frac{1}{V_{P_g}^2} - \frac{1}{V_{P_n}^2}}, \quad (5)$$

where h is crustal thickness, V_{P_g} is crustal P_g velocity, and V_{P_n} is mantle P_n velocity. Using the values from Figure 4, we compute a crustal thickness of 20.6 km. This result is consistent with receiver function results obtained from the Earthscope Automated Receiver Survey (EARS) at the Incorporated Research Institutions in Seismology (IRIS) Data Management Center (DMC) for the USGS Global Seismographic Network (GSN) station CU.SDDR (Fig. 1a; \textcircled{E} Table S1, available in the electronic supplement to this paper) in the Dominican Republic after the methods of [Crotwell and Owens \(2005\)](#), which suggest a crustal thickness of 20 km and crustal velocity of 6.6 km/s. Our observed average crustal P_g velocity of 6.6 km/s is quite fast for a tectonic region, and the crustal thickness of 20 km is very thick for an oceanic environment. The crust in this region, from eastern Cuba to eastern Puerto Rico (Fig. 1), is made up of both exposed islands and shallow ocean depths. Thickened island arc ocea-

20

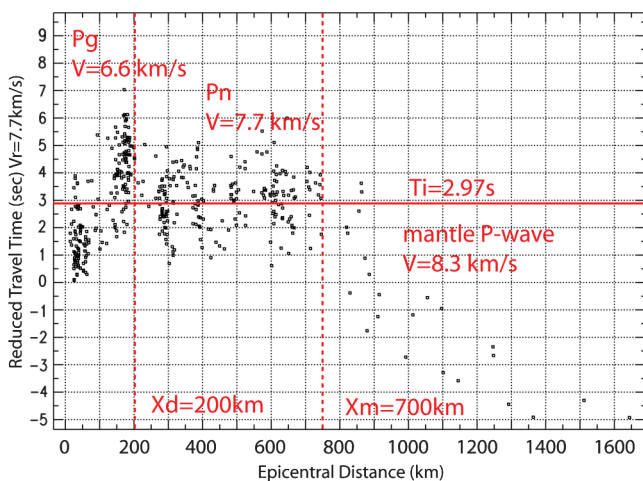


Figure 4. First arriving P -wave travel times plotted with a reducing velocity of 7.7 km/s.

nic crust, due to active collision tectonics along the north plate boundary (Mann *et al.*, 1984), is consistent with our observations of fast P -wave velocity and thick oceanic crust, as well as shallow bathymetry. 21

The crustal structure determined from local and regional distance first arriving P waves is roughly consistent with the path-length dependent S -wave and L_g amplitudes observed in Figure 3. At distances <100 km, crustal waves (P_g and S_g) dominate the seismogram. At distances from 100 to 250 km, L_g develops while both crustal P and S waves are still present. Beyond 200–250 km, body waves consist of small amplitude mantle head waves (P_n and S_n) and crustal L_g dominate the seismogram. Based on these observations, we invert separately for $Q(f)$ using direct S waves at distances <100 km, assuming R^{-1} , and L_g at distances of 250–700 km, assuming $R^{-0.5}$. The hinge point positions for Haiti and the Hispaniola region are unique. However, we use geometric spreading functions consistent with those of previous studies in the region ([Atkinson, 2004](#); [Motazedian and Atkinson, 2005](#)).

Results

L_g Q Results

Vertical component L_g amplitudes, measured in five frequency bands and corrected for the source (S_j), and receiver (G_i) terms are shown in Figure 5. The straight lines represent the best fitting Q for the particular frequency band from equation 3. In each frequency band the inversion procedure solves for an average Q using 749 high-quality L_g amplitude observations from 126 events recorded at 25 stations with a distance range of 250–700 km (Fig. 5). \textcircled{E} Horizontal component L_g amplitudes, measured in five frequency bands and corrected for the source (S_j), and receiver (G_i) terms are available as an electronic supplement to this paper (see Figs. S2 and S3).

S -Wave Q Results

\textcircled{E} Horizontal component S -wave amplitudes, measured in five frequency bands and corrected for the source (S_j), and receiver (G_i) terms are available as an electronic supplement to this paper in Figure S4. The straight lines represent the best fitting Q for the particular frequency band from equation 3. In each frequency band, the inversion procedure solves for an average Q using 90 high-quality S -wave amplitude observations from 22 events recorded at 11 stations with a distance range of 25–80 km (\textcircled{E} see Fig. S4, available in the electronic supplement to this paper).

$Q(f)$ Results

By repeating the inversion over five octaves, with center frequencies of 0.75, 1.5, 3, 6, and 12 Hz, we obtain a Q estimate for each passband. A weighted $L1$ norm least-squares regression analysis is then used to fit the frequency-dependent

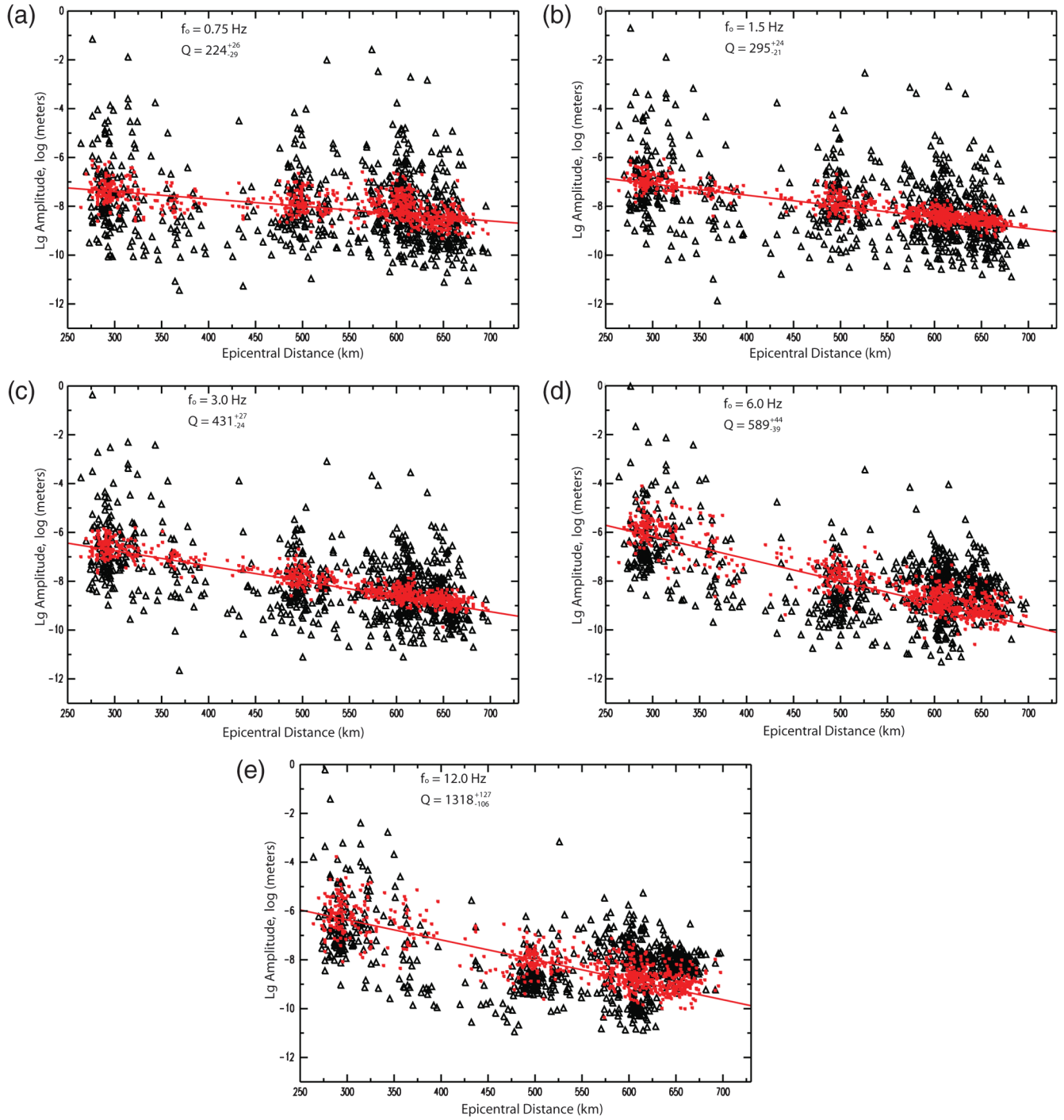


Figure 5. Original vertical component (stations SHZ, HHZ, and BHZ) L_g amplitudes (black triangles) corrected for source and receiver terms determined in the Q inversion (red squares) (a) 0.75 Hz L_g Q results. (b) 1.5 Hz L_g Q results. (c) 3.0 Hz L_g Q results. (d) 6.0 Hz L_g Q results. (e) 12.0 Hz L_g Q results using vertical components.

Q function $Q(f)$, equation (1), to the Q estimates. Taking the logarithm of both sides of equation (1) yields

$$\ln Q = \ln Q_0 + \eta \ln(f) - \eta \ln(f_0), \quad (7)$$

where Q_0 and η are the unknowns to be determined.

22 We find $L_g Q(f) = 245(\pm 31)f^{0.61(\pm 0.082)}$ for the vertical

paper) and for the horizontal components of motion (BHE, HHE, SHE, and BH1) $Q(f) = 228(\pm 27)f^{0.65(\pm 0.081)}$ (see Fig. S6, available in the electronic supplement to this paper) (BHN, HHN, SHN, and BH2) $Q(f) = 220(\pm 21)f^{0.62(\pm 0.064)}$ (see Fig. S7, available in the electronic supplement to this paper). Finally, we combine all horizontal components and determine an average $Q(f) =$

$224(\pm 27)f^{0.64(\pm 0.073)}$, which is the final $L_g Q(f)$ model presented in this analysis. We observe that $L_g Q(f)$ estimated at regional distances is very consistent across vertical and horizontal components. It is interesting to note that the simple SVD linear model fits $L_g Q$ values in the midfrequencies, however at both low and high frequencies, Q values are generally higher than that of the model, suggesting that η steepens with increasing frequency (Fig. 6; see Figs. S6 and S7, available in the electronic supplement to this paper). This has also been observed in previous studies in the continental United States (Erickson *et al.*, 2004) and suggests that more complex modeling may be required. In addition to $L_g Q(f)$, we find $Q(f) = 142(\pm 21)f^{0.71(\pm 0.11)}$ using only horizontal component direct S waves at local distances ≤ 100 km (see Fig. S8, available in the electronic supplement to this paper). For comparison, $Q(f)$ results for all L_g components and the direct S wave are shown in Figure 7.

Error and Resolution

We examined the mean and standard deviation of Q for each region for all frequencies by resampling the original dataset using the delete- j jackknife resampling technique modeled after the method of Efron and Tibshirani (1993). To achieve consistency for the jackknife estimate of standard deviation, we left out at least $d = \sqrt{n}$, where n is the total number of observations and d is the number of observations removed from the complete dataset. To obtain an error bound, we removed d number of randomly selected observations from the total n number of observations to create 1000 new jackknife datasets, and then inverted each jackknife dataset to determine 1000 Q values. From these 1000

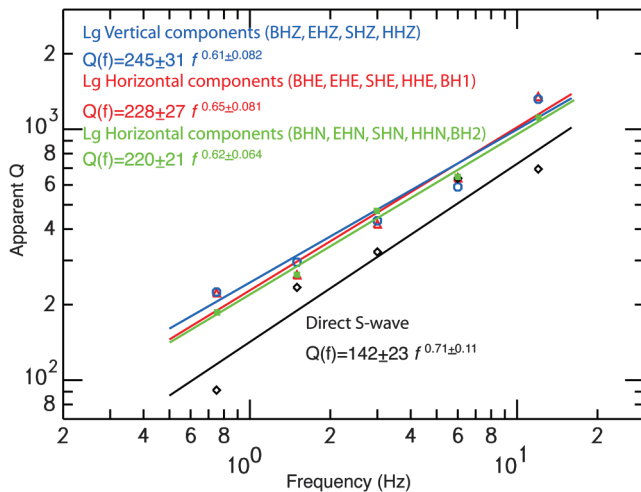


Figure 6. Frequency-dependent $L_g Q(f)$ for vertical components of motion (red) $Q(f) = 245(\pm 31)f^{0.61(\pm 0.082)}$ and horizontal components of motion (blue; stations BHE, HHE, SHE, and BH1) $Q(f) = 228(\pm 27)f^{0.65(\pm 0.081)}$ (green; stations BHN, HHN, SHN, and BH2) $Q(f) = 220(\pm 21)f^{0.62(\pm 0.064)}$. Also shown is the direct S -wave (black) $Q(f) = 142(\pm 21)f^{0.71(\pm 0.11)}$.

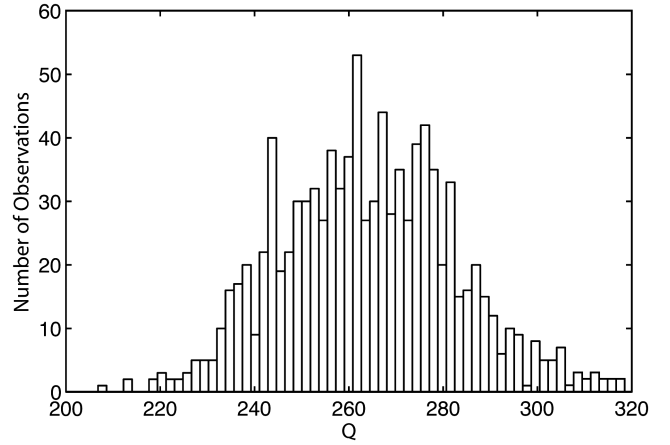


Figure 7. Histogram of 1000 jackknife Q inversions for horizontal component L_g amplitudes at 1.5 Hz. In this example, the total number of observations (n) = 742 and the number of observations removed for each jackknife inversion (d) = 148 are shown. Note the normal distribution of Q values. From 1000 randomly sampled datasets, the average jackknife Q value is 264.25 ± 19.78 .

values, we calculate a standard deviation (2σ) and a mean value for the region at a desired frequency. We then compared the mean Q from the 1000 jackknife datasets to the Q computed from the entire dataset to test for stability and accuracy.

Figure 7 shows a histogram of the results obtained from 1000 different inversions of randomly selected jackknife datasets using the horizontal (SHE, HHE, BHE, and BH1) L_g amplitudes measured in the 0.5–1.0 Hz band (center frequency = 1.5 Hz). We randomly removed 20% of the observations from the complete dataset ($n = 742$) to create 1000 new jackknife datasets, and then inverted each new reduced dataset to obtain 1000 Q values. The mean and standard deviation were calculated from this set of 1000 Q values to establish error estimates for the region. In this example, Q computed from the complete dataset is 262.56 (see Fig. S2b available in the electronic supplement to this paper). After 1000 randomly sampled datasets, with a 20% reduction in the number of data points, the average jackknife Q value is 264.25 ± 19.78 , a difference of only 1.75 from the Q determined from the complete dataset.

We also tested the stability of our datasets by removing an increasing number of waveforms to determine at which point the inversion becomes unstable, and Q is no longer well resolved. Our results remain stable, with a standard deviation less than 50 and a ΔQ less than 50, until about 75% of the data are removed (Fig. 8). This suggests that Q can be determined with relatively few observations and that adding more observations merely decreases the error. Since the variation of Q from the different datasets likely represents the regional variability of the Q structure, these observations reinforce our confidence that our Q results are stable estimates of the frequency-dependent regional average attenuation structure.

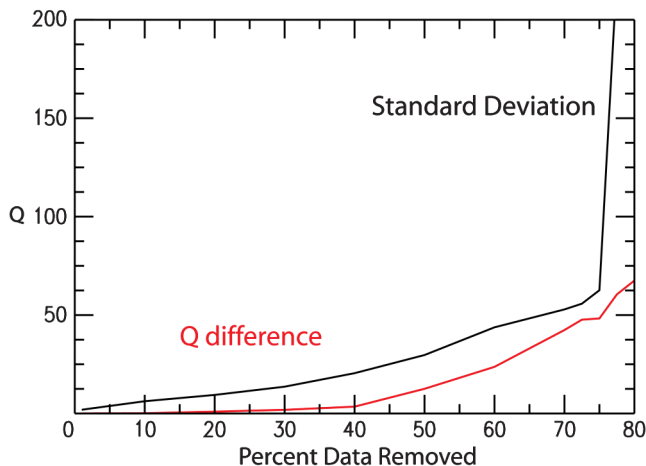


Figure 8. In this plot we show the difference between the average Q determined from 1000 jackknife datasets and the Q inverted from the original complete dataset (red line) versus the percent of data removed. Data are the same as used in Figure 8. Note that the Q difference is very low until 40% of the data are removed. The Q difference gradually increases as an increasing percentage of data are removed. The black line is the standard deviation of the jackknifed Q result versus the percent of data removed from the original dataset before inversion. Note the standard deviation gradually increases until about 75 percent of the original data are removed.

Discussion

Our results show that the attenuation properties of L_g differ from those of the direct S wave in Hispaniola. Differences reflect a depth dependence of attenuation: the L_g waveform samples the entire crust, including the deeper crust, which is likely to be characterized by lower attenuation (higher Q ; Hough and Anderson, 1988), while the direct S waves are more strongly controlled by the upper crust.

Both direct S and L_g $Q(f)$ results for Hispaniola can be compared with results determined for other regions. Of the regions for which L_g attenuation has been investigated, the regional L_g $Q(f)$ results from this study are most similar to the Basin and Range and south-central Alaska (McNamara, 2000; Erickson *et al.*, 2004). The direct S -wave $Q(f)$ estimated in this study is most similar to previous results from southern California. In addition, Raof *et al.* (1999) found $Q(f) = 180f^{0.45}$ for southern California using local S waves, and Frankel *et al.* (1990) computed $Q = 110$ at 3 Hz for southern California, using a geometric spreading function of R^{-1} . The local attenuation properties of Hispaniola, computed in this study, are thus consistent with values estimated for other tectonically active regions.

The nearest region to our study is Puerto Rico (Fig. 9), for which Motazedian and Atkinson (2005) estimate $Q(f) = 359f^{0.59}$ using earthquakes as deep as 200 km. The frequency dependence of our results and Puerto Rico are similar; however Q_0 is lower in our study. The difference between Q_0 in Puerto Rico and in the Hispaniola region might reflect several factors including regional variability in attenuation and the selection of only shallow crustal earthquakes in this study.

Despite the large number of ocean paths traversing the Caribbean Sea surrounding the island of Hispaniola, L_g is generally observed to propagate efficiently and is well observed on seismograms. It is interesting to note that while our observed L_g $Q(f)$ is relatively low and indicative of an active tectonic region, L_g amplitudes are significantly higher than might be expected in an oceanic environment (Zhang and Lay, 1995; McNamara and Walter, 2001). For the Hispaniola region of the Caribbean Sea considered in this study (Fig. 1), the L_g wave train is well developed, suggesting the presence of continental crust. However, L_g paths in this study traverse areas of shallow ocean bathymetry associated with thickened ocean arc crust at the active boundary between the North American and Caribbean tectonic plates (Fig. 1), as opposed to thin oceanic crust, which is typically associated with deeper bathymetry (for a more detailed map of the region see Tarr *et al.*, 2010). In addition to the quantitative $Q(f)$ results presented here, we note that L_g propagation is not exclusive to continental regions but can also propagate in thickened oceanic crust. Because of the complex nature of the crust, we expect that Q will be highly variable throughout other parts of the Caribbean region. Future work will consider Q and L_g propagation for the broader region using previously established tomographic methods (McNamara and Walter, 2001; Pasyanos *et al.*, 2009).

Computing region-specific $Q(f)$ is important to simulating the strong ground shaking for large earthquake scenarios for hazard mitigation planning and for the improvement of probabilistic assessments of seismic hazard, such as the USGS national seismic hazard maps that are used for seismic provisions in building codes (Frankel *et al.*, 2000; Frankel *et al.*, 2002; Petersen *et al.*, 2008). Attenuation characteristics are also important for magnitude detection threshold

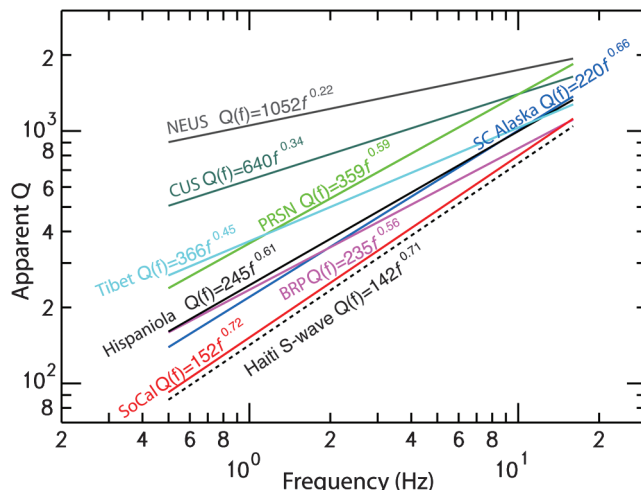


Figure 9. $Q(f)$ results from this study compared to results from numerous regions. The northeastern US (NEUS; Benz *et al.*, 1997), central US (CUS; Erickson *et al.*, 2004), Tibet (McNamara *et al.*, 1996), Puerto Rico (PRSN; Motazedian and Atkinson, 2005), south-central Alaska (McNamara, 2000), Basin and Range (BRP; Benz *et al.*, 1994), and southern California (SoCal, Erickson *et al.*, 2004).

models computed to optimize seismic network design for earthquake and tsunami monitoring (McNamara *et al.*, 2008). This is a first contribution on the understanding of attenuation parameters in the Haiti–Hispaniola region. Additional work such as detailed microzonation, near surface velocity profiling for V_{S30} , and regional phase propagation modeling are required to further improve our understanding of the ground-motion characteristics of the Haiti–Hispaniola region.

Conclusions

In this study we find that L_g propagates well in an ocean environment where the oceanic crust is thickened at an active tectonic boundary and determined frequency-dependent $Q(f)$ for the Hispaniola region using direct S and L_g waves over five distinct passbands from 0.5–16 Hz. For the distance range 250–700 km, we estimate an average frequency-dependent $Q(f) = 224(\pm 27)f^{0.64(\pm 0.073)}$ using horizontal L_g components. We also determine a $Q(f) = 142(\pm 21)f^{0.71(\pm 0.11)}$ for direct S waves at local distances— ≤ 100 km. $Q(f)$ computed in this study is consistent with that determined in other studies in the region and is expected for a tectonically active environment.

Data and Resources

The waveforms used in this study include both horizontal and vertical components of motion from crustal earthquakes recorded at local and regional distances. Events analyzed include the devastating **M** 7.0 Haiti earthquake of 12 January 2010 and the rich sequence of aftershocks (Fig. 1; ㉔ see Table S1, available in the electronic supplement to this paper). All waveforms were visually inspected and restricted to well-recorded (**M** ≥ 2.5) crustal earthquakes (depth ≤ 15 km). Data used in this study were digitally recorded at regional broadband stations operated by the Puerto Rico Seismic Network (PRSN) (Clinton *et al.*, 2006; Pujols, 2008), the seismic network in the Dominican Republic, the USGS GSN (McNamara *et al.*, 2006), and the Canadian National Network. In addition, 10 portable stations were deployed shortly after the Haiti **M** 7.0 earthquake (Hough *et al.*, 2010) (Fig. 1; ㉔ see Table S2, available in the electronic supplement to this paper). Earthquake locations and magnitudes used in this study were obtained from the USGS Preliminary Determination of Epicenters (PDE). All waveform data, from both portable and permanent seismic stations, used in this study are archived and available for download from the IRIS DMC. Analysis and mapping software used includes SAC (Goldstein and Snoke, 2005), GMT (Wessel and Smith, 1991), and Matlab.

Acknowledgments

The authors would like to thank Gari Mayberry, USGS-OFDA, for coordinating this international effort. We are indebted to Austin Volny of Haiti-BME for local support and technical assistance. We would like to

thank G Hayes, J. Boatwright, and R Briggs for helpful discussions. Thoughtful comments were provided by V. Tsai, M. Petersen, Bill Walter and one anonymous BSSA reviewer.

References

- Aki, K. (1980). Scattering and attenuation of shear waves in the lithosphere, *J. Geophys. Res.* **85**, 6496–6504, doi [10.1029/JB085iB11p06496](https://doi.org/10.1029/JB085iB11p06496).
- Atkinson, G. M. (2004). Empirical attenuation of ground motion spectral amplitudes in southeastern Canada and the northeastern United States, *Bull. Seismol. Soc. Am.* **94**, 1079–1095.
- Atkinson, G. M., and D. M. Boore (1995). Ground-motion relations for eastern North America, *Bull. Seismol. Soc. Am.* **85**, 17–30.
- Atkinson, G., and R. Mereu (1992). The shape of ground motion attenuation curves in southeastern Canada, *Bull. Seismol. Soc. Am.* **82**, 2014–2031.
- Aster, R., B. Borchers, and W. Thurber (2002). *Parameter Estimation and Inverse Problems*, Elsevier, Amsterdam.
- Benz, H., A. Frankel, and D. Boore (1997). Regional L_g attenuation for the continental United States, *Bull. Seismol. Soc. Am.* **87**, 606–619.
- Bird, P. (2003). An updated digital model of plate boundaries, *Geochem., Geophys., Geosyst.* **4**, 52, doi [10.1029/2001GC000252](https://doi.org/10.1029/2001GC000252).
- Boore, D. M. (1983). Stochastic simulation of high-frequency ground motions based on seismological models of the radiated spectra, *Bull. Seismol. Soc. Am.* **73**, 1865–1894.
- Calais, E., A. Freed, G. Mattioli, F. Amelung, S. Jónsson, P. Jansma, T. Dixon Sang-Hoon Hong, C. Pèpètit, and R. Momplaisir (2010). Transpressional rupture of an unmapped fault during the 2010 Haiti earthquake, *Nat. Geosci.* **3**, 794–799, doi [10.1038/ngeo992](https://doi.org/10.1038/ngeo992).
- Chavez, D., and K. Priestly (1986). Measurement of frequency dependent L_g attenuation in the Great Basin, *Geophys. Res. Lett.* **13**, 551–554, doi [10.1029/GL013i006p00551](https://doi.org/10.1029/GL013i006p00551).
- Clinton, J. F., G. Cua, V. Huérfano, C. von Hillebrandt-Andrade, and J. Martínez-Cruzado (2006). The current state of seismic monitoring in Puerto Rico, *Seismol. Res. Lett.* **77**, no. 5, 532–543, doi [10.1785/gssrl.77.5.532](https://doi.org/10.1785/gssrl.77.5.532).
- Crotwell, H. P., and T. J. Owens (2005). Automated receiver function processing, *Seismol. Res. Lett.* **76**, no. 6, 702–709, doi [10.1785/gssrl.76.6.702](https://doi.org/10.1785/gssrl.76.6.702).
- Dobrin, M. B., and C. H. Savit (1988). *Introduction to geophysical prospecting*, Fourth Ed., McGraw-Hill, New York, 867 pp.
- Efron, B., and R. J. Tibshirani (1993). *An introduction to the Bootstrap*, Chapman and Hall, in Monographs on Statistics and Applied Probability, Chapman and Hall, London, 57 pp.
- Erickson, D., D. E. McNamara, and H. M. Benz (2004). Frequency dependent L_g Q within the continental United States, *Bull. Seismol. Soc. Am.* **94**, no. 5, 1630–1643, doi [10.1785/012003218](https://doi.org/10.1785/012003218).
- Frankel, A. (1991). Mechanisms of seismic attenuation in the crust: Scattering and anelasticity in New York state, South Africa and, southern California, *J. Geophys. Res.* **96**, 6269–6289.
- Frankel, A., S. Harmsen, C. Mueller, E. Calais, and J. Haase (2010). Documentation for initial seismic hazard maps for Haiti, *USGS Open-File Report 2010-1067*, 12 pp.
- Frankel, A., and L. Wenerberg (1987). Energy-flux model of seismic coda: Separation of scattering and intrinsic attenuation, *Bull. Seismol. Soc. Am.* **77**, 1223–1251.
- Frankel, A., A. McGarr, J. Bicknell, J. Mori, L. Seeber, and E. Cranswick (1990). Attenuation of high-frequency shear waves in the crust: Measurements from New York state, South Africa and, southern California, *J. Geophys. Res.* **95**, 17,441–17,457.
- Frankel, A. D., C. S. Mueller, T. P. Barnhardt, E. V. Lyendecker, R. L. Wesson, S. C. Harmsen, F. W. Klein, D. M. Perkins, N. C. Dickman, S. L. Hanson, and M. G. Hopper (2000). USGS national seismic hazard maps, *Earthq. Spectra* **16**, 1–19, doi [10.1193/1.1586079](https://doi.org/10.1193/1.1586079).
- Frankel, A. D., M. D. Petersen, C. S. Mueller, K. M. Haller, R. L. Wheeler, E. V. Lyendecker, R. L. Wesson, S. C. Harmsen, C. H. Cramer, D. M. Perkins, and K. S. Rukstales (2002). Documentation for the

- 2002 update of the national seismic hazard maps, *USGS Open-file report 02-420*, 33 pp.
- Goldstein, P., and A. Snoko (2005). SAC availability for the IRIS community, *DMS Electronic Newsletter* 7, no. 1: available at <http://www.iris.edu/news/newsletter/vol7no1/page1.htm>.
- 27 Gregersen, S. (1984). L_g wave propagation and crustal structure differences near Denmark and the North Sea, *Geophys. J. Int.* **79**, 217–234, doi [10.1111/j.1365-246X.1984.tb02852.x](https://doi.org/10.1111/j.1365-246X.1984.tb02852.x).
- Gutenberg, B. (1955). Channel waves in the Earth's crust, *Geophysics* **20**, 283–294, doi [10.1190/1.1438141](https://doi.org/10.1190/1.1438141).
- Hayes, G. P., R. W. Briggs, A. Sladen, E. J. Fielding, C. Prentice, K. Hudnut, P. Mann, F. W. Taylor, A. J. Crone, R. Gold, T. Ito, and M. Simons (2010). Complex rupture during the 12 January 2010 Haiti earthquake, *Nat. Geosci.* **3**, 800–805, doi [10.1038/ngeo977](https://doi.org/10.1038/ngeo977).
- Hornbach, M. J., N. Braudy, R. W. Briggs, M. Cormier, M. B. Davis, J. B. Diebold, N. Dieudonne, R. Douilly, C. Frohlich, S. P. S. Gulick, H. E. Johnson III, P. Mann, C. McHugh, K. Ryan-Mishkin, C. S. Prentice, L. Seeber, C. C. Sorlien, M. S. Steckler, S. J. Symithe, F. W. Taylor, and J. Templeton (2010). High tsunami frequency as a result of combined strike-slip faulting and coastal landslides, *Nat. Geosci.* **3**, 783–788, doi [10.1038/ngeo975](https://doi.org/10.1038/ngeo975).
- Hough, S. E., and J. G. Anderson (1988). High-frequency spectra observed at Anza, California: Implications for Q structure, *Bull. Seismol. Soc. Am.* **78**, 692–707.
- Hough, S. E., J. R. Altidor, D. Anglade, D. Given, M. Guillard Janvier, J. Z. Maharrey, M. Meremonte, B. Saint-Louis Mildor, C. Prepetit, and A. Yong (2010). Localized damage caused by topographic amplification during the 12 January 2010 M 7.0 Haiti earthquake, *Nat. Geosci.* **3**, 778–782, doi [10.1038/ngeo988](https://doi.org/10.1038/ngeo988).
- Isacks, B. L., and C. Stephens (1975). Conversion of S_n to L_g at a continental margin, *Bull. Seismol. Soc. Am.* **65**, 235–244.
- Joshi, A., and S. Midorikawa (2004). A simplified method for simulation of strong ground motion using finite rupture model of the earthquake source, *J. Seismol.* **8**, 467–484, doi [10.1007/s10950-004-1595-z](https://doi.org/10.1007/s10950-004-1595-z).
- Kennett, B. (1986). L_g waves and structural boundaries, *Bull. Seismol. Soc. Am.* **76**, 1133–1141.
- Knopoff, L., F. Schwab, and E. Kaussel (1973). Interpretation of L_g , *Geophys. J. Int.* **33**, 389–404, doi [10.1111/j.1365-246X.1973.tb02375.x](https://doi.org/10.1111/j.1365-246X.1973.tb02375.x).
- Manaker, D. M., E. Calais, A. M. Freed, S. T. Ali, P. Przybylski, G. Mattioli, P. Jansma, C. Prepetit, and J. B. De Chaballier (2008). Interseismic plate coupling and strain partitioning in the northeastern Caribbean, *Geophys. J. Int.* **174**, 889–903, doi [10.1111/j.1365-246X.2008.03819.x](https://doi.org/10.1111/j.1365-246X.2008.03819.x).
- McNamara, D. E. (2000). Frequency dependent L_g attenuation in south-central Alaska, *Geophys. Res. Lett.* **27**, 3949–3952, doi [10.1029/2000GL011732](https://doi.org/10.1029/2000GL011732).
- McNamara, D., and W. Walter (2001). Mapping crustal heterogeneity using L_g propagation efficiency throughout the Middle East, Mediterranean, southern Europe and northern Africa, *Pure Appl. Geophys.* **158**, 1165–1188, doi [10.1007/PL00001219](https://doi.org/10.1007/PL00001219).
- McNamara, D., T. Owens, and W. Walter (1996). Propagation characteristics of L_g across the Tibetan Plateau, *Bull. Seismol. Soc. Am.* **86**, 457–469.
- McNamara, D., J. McCarthy, and H. Benz (2006). Improving earthquake and tsunami warning for the Caribbean Sea, Gulf of Mexico and the Atlantic coast, *U.S. Geol. Surv. Fact Sheet 2006-3012*, 4 pp: available at <http://pubs.usgs.gov/fs/2006/3012/> (last accessed).
- 28 McNamara, D. E., Christa von Hillebrandt-Andrade, P. Earle, and R. Buland (2008). Seismic capabilities of an international Caribbean tsunami warning system, *Seismol. Res. Lett.* **80**, no. 2, 344.
- 29 Mitchell, B. J. (1975). Regional Rayleigh wave attenuation in North America, *J. Geophys. Res.* **80**, 4904–4916.
- 30 Mitchell, B. J. (1981). Regional variation and frequency dependence of Q_β in the crust of the United States, *Bull. Seismol. Soc. Am.* **71**, 1531–1538.
- 31 Menke, W. (1980). *Geophysical Data Analysis: Discrete Inverse Theory* Academic Press, San Diego, California.
- Motazedian, D., and G. Atkinson (2005). Ground-motion relations for Puerto Rico, in *Active tectonics and seismic hazards of Puerto Rico, the Virgin Islands, and offshore areas*, P. Mann (Editor), Geol. Soc. Am. Special Paper 385, 61–80.
- Nuttli, O., G. Bollinger, and D. Griffiths (1979). On the relation between modified mercalli intensity and body wave magnitude, *Bull. Seismol. Soc. Am.* **69**, 893–910.
- 32 Oliver, J., and M. Ewing (1957). Higher mode surface waves and their bearing on the Earth's mantle, *Bull. Seismol. Soc. Am.* **47**, 187–204.
- Ottomoller, L. (2002). L_g wave Q tomography in Central America, *Geophys. J. Int.* **150**, 295–302, doi [10.1046/j.1365-246X.2002.01715.x](https://doi.org/10.1046/j.1365-246X.2002.01715.x).
- Pasyanos, M. E., E. M. Matzel, W. R. Walter, and A. J. Rodgers (2009). Broad-band L_g attenuation modeling in the Middle East, *Geophys. J. Int.* **177**, 1166–1176, doi [10.1111/j.1365-246X.2009.04128.x](https://doi.org/10.1111/j.1365-246X.2009.04128.x).
- 33 Petersen, M. D., A. D. Frankel, S. C. Harmsen, C. S. Mueller, K. M. Haller, R. L. Wheeler, R. L. Wesson, Y. Zeng, O. S. Boyd, D. M. Perkins, N. Luco, E. H. Field, C. J. Wills, and K. S. Rukstales (2008). Documentation for the 2008 update of the United States national seismic hazard maps, *USGS Open-File Report 2008-1128*, 60 pp.
- Prentice, C. S., P. Mann, A. J. Crone, R. D. Gold, K. W. Hudnut, R. W. Briggs, R. D. Koehler, and P. Jean (2010). Seismic hazard of the Enriquillo–Plantain Garden fault in Haiti inferred from palaeoseismology, *Nat. Geosci.* **3**, 789–793, doi [10.1038/ngeo991](https://doi.org/10.1038/ngeo991).
- Press, F., and M. Ewing (1952). Two slow surface waves across North America, *Bull. Seismol. Soc. Am.* **42**, 219–228.
- Raooof, M., R. B. Herrmann, and L. Malagnini (1999). Attenuation and excitation of three-component ground motion in southern California, *Bull. Seismol. Soc. Am.* **89**, 888–902.
- Pujols, R. (2008). Seismic background noise of Puerto Rico, *Master's Thesis*, University of Puerto Rico, Mayaguez.
- Richter, C. (1958). *Elementary Seismology* W. H. Freeman, New York.
- 34 Roy, R. F., D. D. Blackwell, and E. R. Decker (1972). , in *The Nature of the Solid Earth*, E. C. Robertson (Editor), McGraw-Hill, New York, 506–543.
- 35 Tarr, A. C., S. Rhea, G. Hayes, A. Villaseñor, K. P. urlong, and H. Benz (2010). Seismicity of the earth 1900–2007, Caribbean plate and vicinity, *U.S. Geol. Surv. Open-File Rept. 2010-1083-A*, scale: 1:8,000,000; available at <http://pubs.usgs.gov/of/2010/1083/a/>.
- Wessel, P., and W. Smith (1991). Free software helps display data, *Eos Trans. AGU* **72**, 445–446, doi [10.1029/90EO00319](https://doi.org/10.1029/90EO00319).
- Xie, J., and B. J. Mitchell (1993). L_g coda Q across Eurasia, in *Yield and Discrimination Studies in Stable Continental Regions*, Mitchell, B. J. (Editor), Report PLTR- 91-2286, Phillips Laboratory, Hanscom Air Force Base, MA, 77–91.
- 36 Zhang, T., and T. Lay (1995). Why the L_g phase does not traverse oceanic crust, *Bull. Seismol. Soc. Am.* **85**, 1665–1678.
- Zeng, Y., J. G. Anderson, and F. Su (1994). A composite source model for computing realistic synthetic strong ground motions, *Geophys. Res. Lett.* **21**, 725–728, doi [10.1029/94GL00367](https://doi.org/10.1029/94GL00367).

US Geological Survey
1711 Illinois Street
Golden, Colorado 80401

Queries

1. I have tentatively assumed that all authors are affiliated with the USGS in Golden. (1) If this is not correct please provide the affiliation information (institution and address) for each author, and (2) provide additional appropriate information (Earthquake Hazards Program, for example).
2. Please check that we have set the magnitude (M) terms as you desire throughout the article.
3. I revised “Two major crustal transpressional strike-slip fault systems [Manaker et al., 2008; Calais, et al., 2010], posing significant earthquake hazard, run roughly east-west across Hispaniola: the Septentrional fault to the north and the Enriquillo Plantain Garden fault to the south...” to “Two major crustal transpressional strike-slip fault systems—the Septentrional fault to the north and the Enriquillo Plantain Garden fault to the south (Manaker et al., 2008; Calais, et al., 2010)—run roughly east–west across Hispaniola posing a significant earthquake hazard...” Please advise whether your meaning is retained.
4. Please advise whether this citation should be McNamara and Walter, 2001, as I have tentatively assumed, or should it be McNamara *et al.*, 1996; McNamara *et al.*, 2006; or McNamara *et al.*, 2008.
5. (1) Please advise whether the intended citation is Xie and Mitchell (1993) as I have tentatively assumed, or if there is a reference Xie *et al.* (2003) that needs to be added to the reference list. (2) If Xie *et al.* (2003) is the intended citation, please provide a complete reference.
6. Please confirm whether Zhang and Lay (1995) is the correct citation as I have assumed. If there is a Zhang and Lay (1994) that you wish to cite, please provide the complete reference.
7. Please confirm whether RMS means root mean square, as I have tentatively assumed.
8. Please confirm whether this should be McNamara and Walter (2001) as I have tentatively assumed.
9. I modified “Shown is the EHE...” to “Shown is the GS.WSYH.00.EHE...” with the assumption that EHE was used as a shortened representation for station GS.WSYH.00.EHE. Please confirm whether your meaning is retained.
10. (1) Please confirm whether Table S2 is in the electronic supplement to this article. (2) Table S2 is mentioned before Table S1, can these be reordered in the supplement so that Table S1 is mentioned before Table S2?
11. Please confirm whether Table S1 is in the electronic supplement to this article.
12. Please confirm whether this should be McNamara and Walter (2001) as I have tentatively assumed.
13. Please confirm whether this should be Menke (1980) as I have assumed. If there is a Menke (1990) that you wish to cite here, please provide the complete reference.
14. I revised “...the geometrical spreading function by a hinged-trilinear functional form...” to “...the geometrical spreading function as a hinged-trilinear functional form...” Please confirm whether your meaning is retained.
15. In the sentence “Figure 3 shows the distribution of raw horizontal component (BHE, BH1) Lg and S-wave amplitudes, measured in the 1-2 Hz frequency band as a function of distance”, (1) do BHE and BH1 represent seismic stations, as I have tentatively assumed, (2) or are the terms acronyms, which means they need to be defined, or (3) is there another explanation of the terms?
16. For (20100112215310), please provide the date and time of the earthquake in the format like (20 March 2010, 18 h 8 m 8.72 s).
17. For (20100328071617), please provide the date and time of the earthquake in the format like (20 March 2010, 18 h 8 m 8.72 s).
18. I deduced that (20100112215310) represent the time and date of the earthquake. So that I do not introduce an error, please provide the date and time of the earthquake in the format like (20 March 2010, 18 h 8 m 8.72 s).
19. For (20100328071617), please provide the date and time of the earthquake in the format like (20 March 2010, 18 h 8 m 8.72 s).
20. Please confirm whether GSN stands for Global Seismographic Network, which I inserted here at first usage, per BSSA guidelines, rather than later in the article.
21. Please (1) provide a complete reference for Mann *et al.* (1984) or (2) indicate that this citation should be deleted per BSSA guidelines.
22. I understand the sentence to mean that formula $Q(f)=245(+31)f^{0.61(+0.082)}$ is Lg for the vertical components of motion and that the formula $Q(f)=228(\pm 27)f^{0.65(\pm 0.081)}$ is Lg for the horizontal components of motion, but I cannot discern to what the formula $Q(f)=220(\pm 21)f^{0.62(\pm 0.064)}$ nor the acronyms BHN, HHN, SHN, and BH2 apply. Can the sentence be revised to make it clear to the reader the meaning of the third set of acronyms and the third formula?
23. Please confirm whether this should be Benz *et al.* (1997) as I have assumed. If there is a Benz *et al.* (1994) that you wish to cite, please provide the complete reference.
24. Please confirm whether this should be Zhang and Lay (1995) as I have assumed. If there is a Zhang and Lay (1994) that you wish to cite, please provide the complete reference.

25. Please confirm whether this should be Goldstein and Snoke (2005). If there is a Goldstein and Snoke (2002) that you wish to cite, please provide the complete reference.
26. Frankel, A., and L. Wenerberg, (1987) is not referenced in the text. Please (1) indicate where this reference should be cited or (2) indicate that the reference should be removed from the reference list, per BSSA guidelines.
27. Please provide the last accessed date (month and year) for this site.
28. Please provide the last accessed date (month and year) for this site.
29. McNamara, D.E., Christa von Hillebrandt-Andrade, P. Earle, R. Buland does not have a date. Please check this reference. I have been unable to find this article.
30. Mitchell, B. J., (1975) is not referenced in the text. Please (1) indicate where this reference should be cited or (2) indicate that the reference should be removed from the reference list, per BSSA guidelines.
31. Mitchell, B. J., (1981) is not referenced in the text. Please (1) indicate where this reference should be cited or (2) indicate that the reference should be removed from the reference list, per BSSA guidelines.
32. Nuttli, O., G. Bollinger, and D. Griffiths, (1979) is not referenced in the text. Please (1) indicate where this reference should be cited or (2) indicate that the reference should be removed from the reference list, per BSSA guidelines.
33. Pasyanos, M.E., E.M. Matzel, W.R. Walter, and A.J. Rodgers, (2009) is not referenced in the text. Please (1) indicate where this reference should be cited or (2) indicate that the reference should be removed from the reference list, per BSSA guidelines.
34. Richter, C., (1958) is not referenced in the text. Please (1) indicate where this reference should be cited or (2) indicate that the reference should be removed from the reference list, per BSSA guidelines.
35. Roy, R.F., D.D. Blackwell, and E.R. Decker, (1972) is not referenced in the text. Please (1) indicate where this reference should be cited or (2) indicate that the reference should be removed from the reference list, per BSSA guidelines. (3) Please provide the article or chapter title cited for this reference.
36. Xie, J., and B. Mitchell, (1993). Please confirm whether the information added to complete this reference is correct.